Nanoscale

Cite this: *Nanoscale*, 2012, **4**, 1565

www.rsc.org/nanoscale

COMMUNICATION

One-dimensional ferromagnetic dendritic iron wire array growth by facile electrochemical deposition†

Ri Qiu,‡[a] Jin You Zheng,‡[b] Hyun Gil Cha,[b] Myung Hwa Jung,[c] Kyu Joon Lee[c] and Young Soo Kang*[b]

Received 17th November 2011, Accepted 12th January 2012
DOI: 10.1039/c2nr11780k

One-dimensional ferromagnetic iron dendritic wire array film is prepared by facile electrodeposition. The space hindrance effect caused by neighbouring crystals resists the free growth directions parallel to the substrate, which is considered as a possible growth mechanism of one-dimensional morphology. Dendritic iron wire can be transformed into α-Fe_2O_3 without destroying the dendritic morphology by thermal oxidation.

The production of nano- or micro-structured materials with a desired morphology is one of the most challenging tasks in the nano-science and technology fields. Morphology strongly influences the physical and chemical properties of materials. Therefore, a great deal of effort has been devoted to the preparation of materials with different morphologies.[1] Among a variety of shapes in the gallery, one-dimensional material has great utility in the different fields including nanoscale electronics, optoelectronics and molecular sensing.[2] In recent years, versatile approaches have been introduced for the fabrication of one-dimensional materials, such as vapor–liquid–solid (VLS) synthesis[3] and electrodeposition with porous templates, *e.g.*, polycarbonate or anodic aluminium oxide (AAO) membranes.[4] However, these methods require high temperatures and specialized conditions. During the VLS process, metal catalysts (*e.g.*, gold or silver) are necessary and crystal growth occurs at high temperature, typically 500–1200 °C. For the AAO approach, the porous AAO should be prepared and a conductive layer on it is essential. The acid or alkaline treatment is necessary to dissolve the AAO after electrodeposition. Some methods of one-dimensional material fabrication require a complex and tedious purification process.[5]

Nano-scale iron materials have attracted much attention due to their potential magnetic and biomedical applications.[6–11] However, one-dimensional structure is seldom reported. Vayssieres *et al.* showed that one-dimensional iron nanorods can be fabricated by growth of iron oxyhydroxide nanorods onto a single or polycrystalline substrate followed by iron oxyhydroxide reduction to metallic iron in H_2 atmosphere at 300 °C.[9] Up to now, the low-cost and energy-efficient growth of well-aligned one-dimensional iron structure at ambient environment is still a challenge.

Herein, we report a facile way to prepare one-dimensional ferromagnetic iron dendritic wires by electrochemical deposition and iron film can be easily transformed into α-Fe_2O_3 dendritic wires array film by thermal oxidation. The space hindrance effect enforces the iron crystal to grow as a one-dimensional wire, which is composed of three arrays of dendrites. To the best of our knowledge, the detailed mechanism of the iron hierarchical structure growth by electrochemical deposition has not been reported yet.

From our experiments, it has been known that the one-dimensional structure can only be obtained with certain pH and potential values (see S2 and Fig. S1, ESI†). With the deposition of potential −1.25 V to the solution containing 0.05 M $FeSO_4$ and 0.1 M Na_2SO_4 at pH = 2.47 (see S1, ESI†), the reaction of $Fe^{2+} + 2e^- = Fe$ ($E^0 = -0.44$ V *vs.* RHE) will occur irreversibly to achieve a dendritic iron wire array. Fig. 1 shows typical FE-SEM images of the one-dimensional iron wires. Also, the wires clearly exhibit a dendritic profile (Fig. 1c). Large amounts of wires are formed on the surface of the Cu substrate. In Fig. 1a, the aggregation of wires as clusters is due to the capillary effect accompanying the array desiccation process. When the liquid (water or acetone) retaining among the wires evaporates,

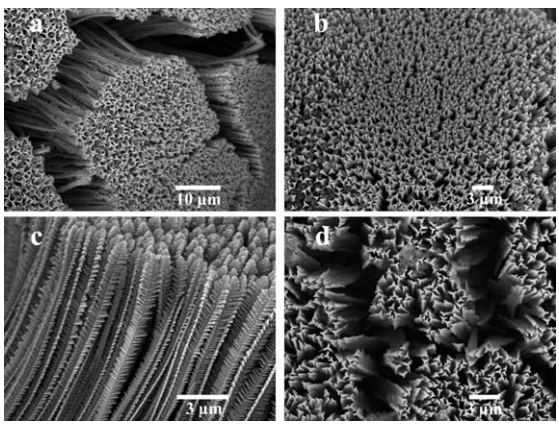

Fig. 1 FE-SEM images of the one-dimensional dendritic iron wire array obtained from electrolysis of a 10 mL aqueous solution containing 0.05 M $FeSO_4$ and 0.1 M Na_2SO_4 at pH 2.47, −1.25 V potential for 600 s. (a and b) Tilted view; (c) profile view; and (d) top view.

[a]*Institute of Oceanology, Chinese Academy of Sciences, 7 Nanhai Road, Qingdao 266071, China*
[b]*Department of Chemistry, Sogang University, Seoul, South Korea. E-mail: yskang@sogang.ac.kr; Fax: +82-2-701-0967*
[c]*Department of Physics, Sogang University, Seoul, South Korea*
† Electronic supplementary information (ESI) available: Experimental details, characterization and Fig. S1–S5. See DOI: 10.1039/c2nr11780k
‡ These authors contributed equally.

the surface tension caused by the capillary effect draws the adjacent wires closer; therefore, clusters are formed and the ravine-like gaps appear. The length of the wires is uniform in large area. From different perspectives such as tilted (a and b), profile (c) and top (d) view, it is observed that the tips of the wires are nearly on the same plane and all wires have triangular cross-sections. The arrays are strictly arranged in order so that only the projected triangular sections are exhibited, as distinguished from Fig. 1d and S2a†. Intuitively, the wire bundle given in Fig. S2b† illustrates that wires have homogeneous length (*ca.* 42 μm). For the delicate structure of a single dendritic wire, high resolution SEM is used to reveal the details. Fig. S3† illuminates the hierarchical characteristic of the one-dimensional wire. Three different locations are sampled for the hierarchical appearance. For Fig. S3b–S3d†, they represent the root, intermediate part and tip of one single wire, respectively. The dendritic wire is composed of a main stem and two ordered branches, which can be identified clearly from Fig. S3c†. The secondary branches are the smallest dendrites below the sub-micron scale to assemble into bigger dendrites (larger than 1 μm), which is regarded as the primary branch of the wire. Every three primary branches overlap the relative adjacent sides and construct a unit of triangle conformation. All these units are piled up along the direction of the main stem to form a dendritic wire. Luckily, this characteristic has been clearly observed in Fig. S3c†. The dendritic wire has three primary branch arrays along three different directions with *ca.* 120° angles, which is of triad axis symmetry. The symmetrical triangle sections can be easily discovered from Fig. 1c and d and S2a†.

The as-obtained deposit is subjected to XRD to reveal the crystal phase. The peaks of XRD patterns (Fig. 2), except the ones corresponding to the Cu substrate, are indexed by JCPDS no. 65-4899. This indicates that the as-obtained material is α-Fe (bcc structure). However, the peak presenting (200) corresponding to $2\theta = 65°$ is absent, which is presumably due to crystal face inhibition during the crystal growth process. Furthermore, with long growth time (30 min), the relative intensity of the peaks compared to the ones of the Cu substrate increases, which indicates that more deposits are obtained.

TEM and SAED are used to reveal the crystal structure of a single dendritic wire, as shown in Fig. 3. The hierarchical structure is manifested prominently by TEM. The vivid primary dendritic branches with hundreds of nanometres are presented in Fig. 3a. Further, the dendrites constructing the branches can also be distinguished. The SAED pattern shown in Fig. 3b suggests single crystalline structure in the edge area. The crystal faces are indexed as (110) and (222), respectively. In the HRTEM image (Fig. 3c), the crystal

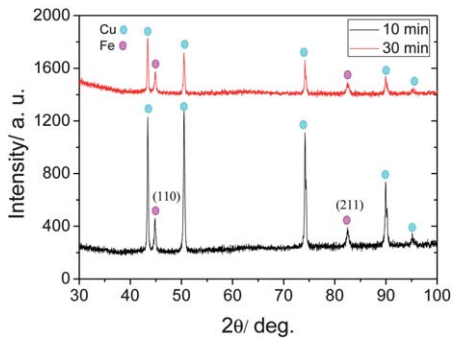

Fig. 2 XRD patterns of α-Fe obtained at a potential of −1.2 V with an electrolysis time of 10 and 30 min.

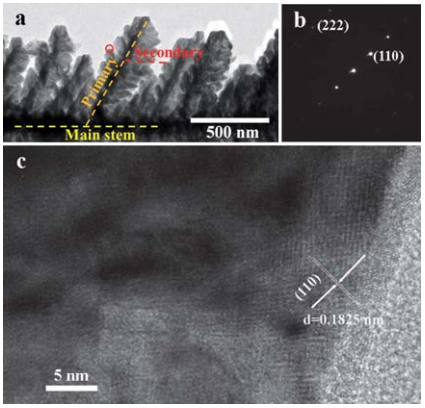

Fig. 3 (a) TEM image of the micron scale wire; (b) the SAED pattern, which is acquired at the marked position of (a); and (c) HRTEM image: the lattice of the (110) crystal face.

lattices are clearly observed and match the (110) crystal face. With the sophisticated techniques, XRD and SAED, it is confirmed that the as-grown dendritic wires are the hierarchical metallic iron.

As a proof out of the element composition, the EDS elemental mapping is devoted to elaborate analysis of the dendrite. The elemental distribution of a partial dendritic wire is shown in Fig. 4. There are two main elements, iron and oxygen, contained in the product. The atomic ratio of Fe to O is ~84 : 16, which proves that the dendritic iron wire consists of either oxide such as Fe_2O_3 or FeOOH. It is assumed that the foreign oxygen reacts with iron when the electrolysis process is completed. Since the nanoscale iron dendrites are very reactive, they will react with water in the aqueous solution or O_2 in the air. During our research, if the black iron material is scratched off the electrode and put into water, the color will change to brown promptly; which indicates that iron oxide or iron hydroxide is formed.

As illustrated in Fig. 5, a possible mechanism based on the space hindrance effect (SHE) is proposed to elucidate the one-dimensional dendritic wire formation process. The ideal space hindrance effect is schematically illustrated in Fig. 5a. At first, the triangular hierarchical structures are formed when the crystals nucleate on the surface of the electrode (Fig. 5b). The elongation of the triangular form is along the direction perpendicular to the substrate. The neighboring dendrites act as walls to block the mass transfer parallel to the substrate, inhibiting the excess elongation along the plane. The crystals are enforced to grow along the perpendicular direction by consuming the precursor in the bulk solution (Fig. 5b), which at last creates one-dimensional wired structures. We call this a space hindrance effect driving crystal growth. The retaining triangular cross-section of the crystal plays an important role in the wired shape formation. Since the triangular structure is naturally stable, each wire can stand firmly

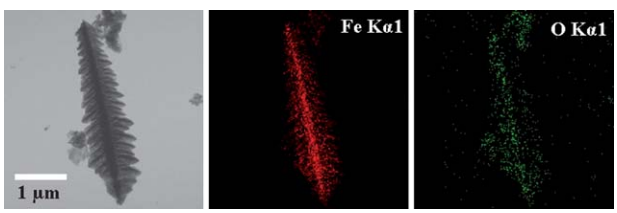

Fig. 4 EDS elemental mapping of the as-achieved iron dendrite.

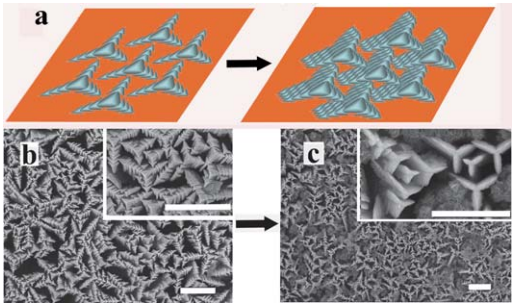

Fig. 5 (a) Schematic illustration of the crystal growth mechanism. (b) FE-SEM image of the triangular dendrites formed during the nucleation process and (c) elongated triangular dendrites. All bars in the figure represent 3 μm.

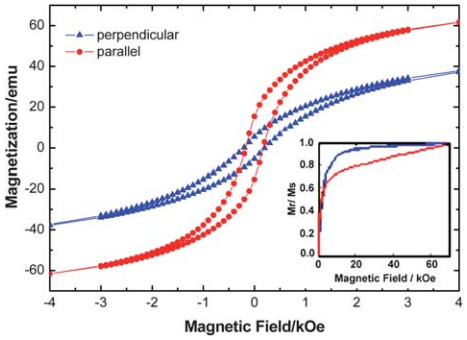

Fig. 6 Parallel and perpendicular hysteresis loops for an iron dendrite wire array at room temperature.

on the electrode; therefore, an array composed of one-dimensional dendritic wires is formed. Moreover, the neighbouring iron wires in the array can surround one-dimensional spaces to form narrow channels (width less than 1 μm in Fig. 5b), which induce high capillary force. The water droplets will spread rapidly and realize superhydrophilicity on the surface of the array (see S3 and Fig. S4, ESI†), which indicates a potential application in thermal engineering and other fields.[12]

Magnetic properties of the dendritic iron wire array are analyzed by magnetization hysteresis loops with magnetic fields parallel and perpendicular to the array surface. As shown in Fig. 6, the hierarchical structure reveals ferromagnetic behavior. An external magnetic field parallel (perpendicular) to the surface is approximately perpendicular (parallel) to the iron wire. Under parallel and perpendicular magnetic fields at room temperature, the corresponding coercivity values are measured as 170 and 210 Oe, respectively. As shown in the inset of Fig. 6, when the external parallel magnetic field is up to 60 kOe, the magnetization of iron dendrite wire is not saturated. However, the trend of magnetization to the saturation state is much faster under a perpendicular magnetic field. The demagnetization is less in the case of a perpendicular field, namely, parallel to the iron dendrite wires, which indicates that the magnetization is along the long axis of iron dendrite wires. It is deduced that the magnetic moments of domain in the iron wire are oriented along the wire axis, resulting in an easy axis of magnetization along the long axis.

In a previous study, Sun *et al.*[13] reported that the α-Fe_2O_3 dendrite could be converted to other chemical states of iron without destroying the external morphology by a redox process. Herein, iron dendrites can be thermally oxidized into a one-dimensional dendritic α-Fe_2O_3 structure, which has been confirmed by XRD and EDS shown in Fig. S5†.

In this work, a one-dimensional dendritic iron wire array is prepared by electrochemical deposition. A strategy based on the space hindrance effect is applied to direct crystal growth to one-dimensional morphology. The as-prepared hierarchical iron illustrates ferromagnetism and superhydrophilicity properties, which enables its potential application in respective fields. Furthermore, the wires are changed into dendritic α-Fe_2O_3, which can be potentially used as a photoelectrode for water splitting. Further studies are still undergoing.

This work was supported by the Korea Center for Artificial Photosynthesis (KCAP) located in Sogang University funded by the Ministry of Education, Science, and Technology (MEST) through the National Research Foundation of Korea (NRF-2009-C1AAA001-2009-0093879).

Notes and references

1 (*a*) A. P. Alivisatos, *Science*, 1996, **271**, 933; (*b*) J. D. Holmes, K. P. Johnston, R. C. Doty and B. A. Korgel, *Science*, 2000, **287**, 1471.
2 (*a*) P. D. Yang, *Nature*, 2003, **425**, 243; (*b*) Y. Huang, X. F. Duan and C. M. Lieber, *Small*, 2005, **1**, 142; (*c*) A. J. Miezawska, R. Jalilian, G. U. Sumanasekera and F. P. Zamborini, *Small*, 2007, **3**, 722.
3 (*a*) J. Hu, T. W. Odom and C. M. Lieber, *Acc. Chem. Res.*, 1999, **32**, 435; (*b*) Y. Wu, H. Yan and P. Yang, *Chem.–Eur. J.*, 2002, **8**, 1260; (*c*) Y. Wu and P. Yang, *J. Am. Chem. Soc.*, 2001, **123**, 3165.
4 F. H. Xue, G. T. Fei, B. Wu, P. Cui and L. D. Zhang, *J. Am. Chem. Soc.*, 2005, **127**, 15348.
5 S. R. C. Vivekchand, R. Jayakanth, A. Govindaraj and C. N. R. Rao, *Small*, 2005, **1**, 920.
6 K. S. Suslick, M. M. Fang and T. H. Hyeon, *J. Am. Chem. Soc.*, 1996, **118**, 11960.
7 S. Peng, C. Wang, J. Xie and S. H. Sun, *J. Am. Chem. Soc.*, 2006, **128**, 10676.
8 K. Somaskandan, T. Veres, M. Niewczas and B. Simard, *New J. Chem.*, 2008, **32**, 201.
9 L. Vayssieres, L. Rabenberg and A. Manthiram, *Nano Lett.*, 2002, **2**, 1393.
10 Y. X. Chen, S. P. Chen, Z. Y. Zhou, N. Tian, Y. X. Jiang, S. G. Sun, Y. Ding and Z. L. Wang, *J. Am. Chem. Soc.*, 2009, **131**, 10860.
11 Y. M. Wei, Y. C. Fu, J. W. Yan, C. F. Sun, Z. Shi, Z. X. Xie, D. Y. Wu and B. W. Mao, *J. Am. Chem. Soc.*, 2010, **132**, 8152.
12 S. J. Kim, I. C. Bang, J. Buongiorno and L. W. Hu, *Appl. Phys. Lett.*, 2006, **89**, 153107.
13 G. Sun, B. Dong, M. Cao, B. Wei and C. Hu, *Chem. Mater.*, 2011, **23**, 1587.